

Less is More: Robust Zero-Communication 3D Pursuit-Evasion via Representational Parsimony

Jialin Ying, Zhihao Li, Zicheng Dong, Guohua Wu and Yihuan Liao*

Department of Automation, Central South University, Changsha, China

Abstract—Asymmetric 3D pursuit–evasion in cluttered voxel environments is difficult under communication latency, partial observability, and nonholonomic maneuver limits. While many MARL methods rely on richer inter-agent coupling or centralized signals, these dependencies can become fragility sources when communication is delayed or noisy. Building on an inherited path-guided decentralized pursuit scaffold [1], we study a robustness-oriented question: can representational parsimony improve communication-free coordination?

We instantiate this principle with (i) a parsimonious actor observation interface that removes team-coupled channels (83-D \rightarrow 50-D), and (ii) Contribution-Gated Credit Assignment (CGCA), a locality-aware credit structure for communication-denied cooperation. In Stage-5 evaluation (4 pursuers vs. 1 evader), our configuration reaches 0.753 ± 0.091 success and 0.223 ± 0.066 collision, outperforming the 83-D FULL OBS counterpart (0.721 ± 0.071 , 0.253 ± 0.089). It further shows graceful degradation under speed/yaw/noise/delay stress tests and resilient zero-shot transfer on urban-canyon maps (about 61% success at density 0.24). These results support a practical design principle: in communication-constrained multi-robot pursuit, representational sparsity may be more robust than richer inter-agent coupling.

Index Terms—multi-agent reinforcement learning, pursuit–evasion, spatiotemporal decoupling, zero communication, sim-to-real robustness

I. INTRODUCTION

3D pursuit–evasion in cluttered voxel spaces is difficult because communication latency, partial observability, and non-holonomic constraints interact with highly non-convex geometry. In the 4-vs-1 setting considered here, pursuers are maneuver-limited ($v_x \leq 8$ m/s, $|\dot{\psi}| \leq 0.8$ rad/s nominally) while the evader reaches 9 m/s in Stage 5, so stale estimates and delayed corrections can destabilize cooperative interception.

A common MARL strategy is to increase inter-agent coupling via richer teammate-conditioned observations, explicit communication, or centralized critics. Although helpful in nominal simulation, these couplings may propagate stale peer beliefs under delay/noise. We therefore ask: *does decentralized coordination in complex 3D pursuit necessarily require richer cross-agent coupling?*

Reference [1] introduced the path-guided collaborative search-and-capture scaffold (3D A* guidance + directional frontier allocation). Rather than revisiting that scaffold design,

this paper studies a different question: which observation and credit structures remain robust under communication denial, delay, and sensing noise in cluttered 3D pursuit–evasion? We treat the inherited learner as a parameter-shared decentralized PPO/IPPO-style actor–critic (as implemented in [1]), distinct from centralized-critic MAPPO variants.

Our core insight is a robustness-oriented design principle: *representational parsimony can improve communication-free coordination*. Our study highlights two counter-intuitive effects in this regime: (i) more team-coupled information can reduce rather than improve robustness; and (ii) communication-free cooperation can remain strong when sparse local observations are paired with locality-aware credit assignment. Our contributions are:

- **Representational parsimony as a design principle for decentralized MARL in communication-constrained 3D pursuit.** We identify that reducing explicit cross-agent observation coupling can improve robustness under delay and sensing noise.
- **Contribution-Gated Credit Assignment (CGCA).** We introduce a locality-aware credit structure that sustains cooperative capture quality without explicit communication channels.
- **Comprehensive robustness/generalization evidence.** We provide benchmark evaluation plus speed/yaw/noise/delay stress suites and zero-shot transfer on procedurally generated urban-canyon maps.

The macro-topological planning scaffold itself is retained from [1]; our novelty lies in robustness-oriented information and credit design on that inherited decentralized foundation.

II. RELATED WORK

1) *A. 3D Pursuit–Evasion:* Classical pursuit guidance is grounded in analytic controllers such as APF-style reactive potential shaping [12] and proportional navigation (PN) [13]. These methods are lightweight and interpretable, but they are fundamentally local and therefore vulnerable to topological deadlocks in voxelized 3D clutter: the controller can remain trapped in obstacle-induced local minima or oscillatory turn–overshoot cycles. Topology-aware planning (e.g., A*) alleviates some deadlocks by exposing homotopy-level structure [11], yet standalone planning remains brittle under delayed actuation and model mismatch. Recent DRL pipelines improve

*Corresponding author: Yihuan Liao (email: 225189@csu.edu.cn)

adaptability, but naive end-to-end formulations frequently face combinatorial explosion in high-dimensional partially observable state spaces [4]. The path-guided decentralized scaffold of [1] (named PGF-MAPPO in that paper) therefore motivates a pragmatic compromise: a planner encodes global geometry, while the policy specializes in local, uncertainty-aware residual control.

2) *B. Communication-Constrained MARL*: Explicit communication in MARL has been extensively studied through differentiable messaging, attention routing, and graph interaction modules, including CommNet, attentional communication, and targeted multi-agent communication [5]–[8]. In simulation, these channels can improve coordination efficiency; however, high-frequency aerial pursuit is precisely the regime where communication quality is non-stationary. Delay, packet dropout, and asynchronous clocks convert message passing into stale belief propagation, which can trigger cross-agent error cascade rather than cooperation gains. This mismatch becomes especially acute when control horizons are short and collision margins are thin. Our zero-communication actor design is thus not an austerity choice; it is a robustness prior that explicitly severs fragile coupling pathways and forces policy learning to rely on local geometry plus shared topological guidance.

3) *C. Credit Assignment in Cooperative MARL*: Credit assignment remains central in cooperative MARL. Counterfactual baselines such as COMA and value-factorization methods such as VDN/QMIX reduce multi-agent non-stationarity by introducing centralized structure during training [3], [9], [10]. These methods are powerful when global state is reliable, but the dependence on centralized signals can become a practical bottleneck in realistic distributed robotics, where synchronized state aggregation is costly or unavailable. In contrast, CGCA uses only local distance and closing-kinematics signals to shape cooperative incentives. This lightweight locality makes the mechanism naturally compatible with strict decentralized execution and avoids adding another high-dimensional centralized channel on top of already difficult 3D pursuit dynamics.

III. PROBLEM FORMULATION AND ENVIRONMENT SETUP

A. Stage-5 environment

The world is discretized into a $52 \times 52 \times 18$ voxel grid (voxel size: 6.0 m) over $311.0 \times 311.0 \times 110.5$ m. Stage-5 settings include 60 m visibility range, 8 m capture radius, and a 70% visibility gate. The traversable occupancy ratio is 0.127, and the largest free connected component covers 0.951 of free voxels, indicating cluttered but globally navigable topology.

B. Asymmetric game model

Let pursuer $i \in \{1, 2, 3, 4\}$ have position $\mathbf{p}_t^i \in \mathbb{R}^3$, yaw ψ_t^i , and body-frame control

$$\mathbf{u}_t^i = [v_{x,t}^i, v_{y,t}^i, v_{z,t}^i, \dot{\psi}_t^i]^\top. \quad (1)$$

Dynamics are

$$\mathbf{p}_{t+1}^i = \mathbf{p}_t^i + \Delta t \mathbf{R}_z(\psi_t^i) \mathbf{v}_t^i, \quad \psi_{t+1}^i = \psi_t^i + \Delta t \dot{\psi}_t^i, \quad (2)$$

TABLE I
STAGE-5 ENVIRONMENT AND ASYMMETRY CONSTANTS.

Item	Value
World/grid	$311.0 \times 311.0 \times 110.5$ m, $52 \times 52 \times 18$ voxels
Team setup	4 pursuers vs. 1 evader
Capture radius (Stage 5)	8.0 m
Visibility range (Stage 5)	60.0 m
Pursuer bounds	$ v_x \leq 8, v_y \leq 4, v_z \leq 3$ m/s
Pursuer yaw cap	$ \dot{\psi} \leq 0.8$ rad/s (swept down to 0.2)
Evader speed schedule	up to 9.0 m/s
Altitude	occupancy
anisotropy	15.9% / 12.1% / 10.2%

with constraints

$$|v_{x,t}^i| \leq 8, |v_{y,t}^i| \leq 4, |v_{z,t}^i| \leq 3, |\dot{\psi}_t^i| \leq \bar{\omega}. \quad (3)$$

Capture is defined by

$$\min_i \|\mathbf{p}_t^i - \mathbf{p}_t^e\|_2 \leq R_c, \quad R_c = 8 \text{ m}. \quad (4)$$

The cooperative objective is $J(\theta) = \mathbb{E}_{\pi_\theta}[\sum_t \gamma^t r_t]$ with dense collision/safety penalties and capture-quality incentives.

IV. METHODOLOGY

A. Inherited path-guided decentralized scaffold

Following [1], each agent receives a topology-aware 3D A* guidance vector instead of raw path polylines. The planner provides macro free-space structure, while the recurrent policy handles local reactive control. We retain this macro–micro decoupled pursuit scaffold as inherited infrastructure rather than a contribution of the present paper.

For method-boundary clarity, we follow the inherited implementation in [1] as a parameter-shared decentralized PPO/IPPO-style actor–critic, and treat centralized-critic MAPPO variants separately.

B. Observation-space formalization: representational parsimony via 83-D to 50-D masking

Let $\tilde{\delta}_t^i \in \mathbb{R}^{83}$ denote the full actor-side observation for pursuer i at time t :

$$\tilde{\delta}_t^i = [\ell_t^i, \Delta \mathbf{p}_{ie}^t, \Delta \mathbf{v}_{ie}^t, \mathbf{v}_t^i, \mathbf{a}_t^i, \boldsymbol{\omega}_t^i, \phi(\mathcal{N}_i^t), \mathbf{g}_t^i, \mathbf{e}_i, m_t, \delta_t, \mathbf{s}_t^i, \mathbf{c}_t^i], \quad (5)$$

where $\phi(\mathcal{N}_i^t) \in \mathbb{R}^{24}$ encodes top- k teammate states, $\mathbf{s}_t^i \in \mathbb{R}^7$ is the tactical-slot block, and $\mathbf{c}_t^i \in \mathbb{R}^2$ contains encirclement topology cues. To enforce representational parsimony under communication denial, we apply a binary masking operator $\mathbf{M} \in \{0, 1\}^{50 \times 83}$:

$$\boldsymbol{\delta}_t^i = \mathbf{M} \tilde{\boldsymbol{\delta}}_t^i = [\tilde{\boldsymbol{\delta}}_{i,1:41}^t, \tilde{\boldsymbol{\delta}}_{i,66:74}^t] \in \mathbb{R}^{50}. \quad (6)$$

Equivalently, the operator explicitly nulls team-coupled channels,

$$\mathbf{M} \phi(\mathcal{N}_i^t) = \mathbf{0}, \quad \mathbf{M} \mathbf{s}_t^i = \mathbf{0}, \quad \mathbf{M} \mathbf{c}_t^i = \mathbf{0}, \quad (7)$$

thereby removing 24-D teammate states and 9-D slot/encirclement descriptors. This operation is not introduced as generic feature pruning; it explicitly removes team-coupled

Baseline Training Curves (mean \pm ci95)

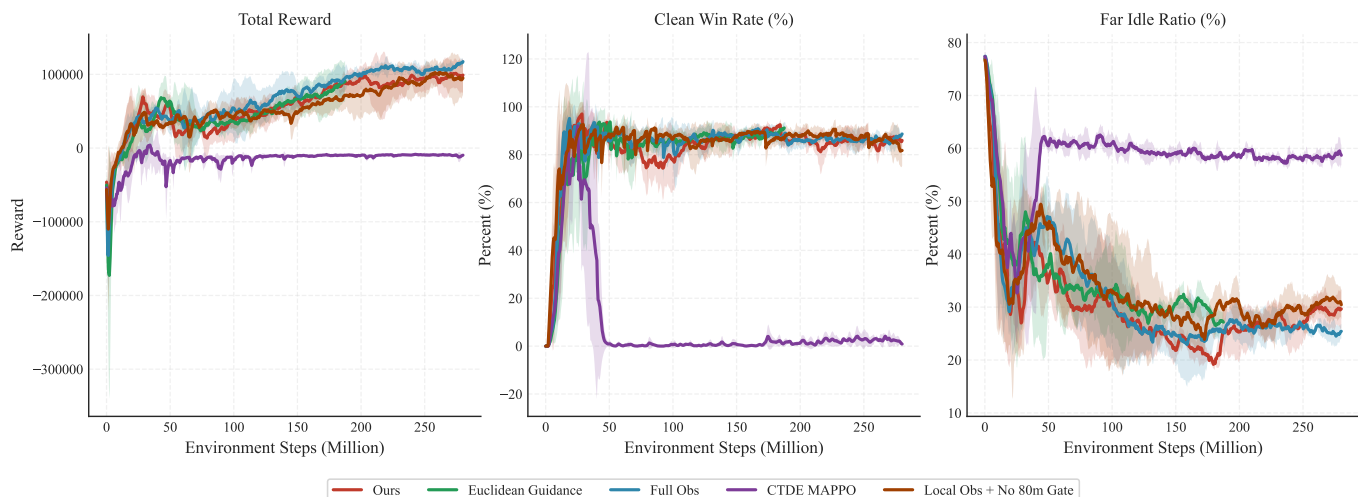


Fig. 1. Training reward curves under Stage 5. CTDE MAPPO shows marked instability after the visibility-gated transition, whereas OURS-LITE converges to the highest stable return regime.

channels that are most vulnerable to stale peer estimates, reducing sensitivity to delay/noise while keeping the action space and optimization backbone unchanged.

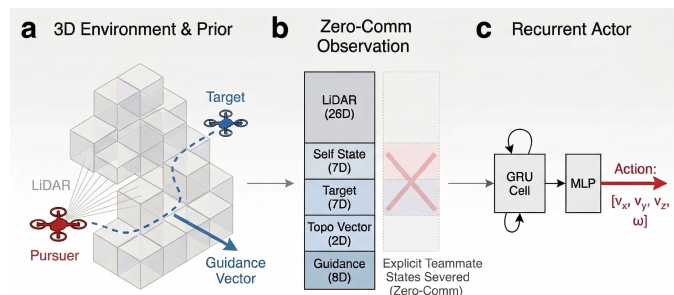


Fig. 2. Inherited path-guided decentralized pipeline [1]. Our change is at the actor interface: 83-D full observation is masked to 50-D by removing teammate/slot/encirclement channels for zero-communication robustness.

TABLE II
OBSERVATION-PROFILE REDUCTION FOR REPRESENTATIONAL PARSIMONY.

Block	83-D	50-D
LiDAR + target + self + IMU	41	41
Teammate top- k	24	0
Guidance + ID + mode + delay	9	9
Slot + encirclement	9	0
Total	83	50

C. Reward composition and Contribution-Gated Credit Assignment (CGCA)

CGCA is designed as a locality-aware credit structure for communication-free cooperation, rather than a generic reward bonus. It rewards geometrically meaningful local participation in interception and suppresses free-rider equilibria when explicit messaging is unavailable.

The cooperative objective for parameters θ is

$$J(\theta) = \mathbb{E}_{\pi_\theta} \left[\sum_{t=0}^T \gamma^t \frac{1}{N_t} \sum_{i=1}^{N_t} r_i^t \right], \quad (8)$$

with per-agent reward decomposition

$$r_i^t = \lambda_{\text{dir}} g_{\text{dir}}(d_i^t) \Delta d_i^t + \lambda_{\text{cap}} \rho^t \hat{c}_i^t \mathbf{1}_{\text{cap}}^t + \lambda_{\text{qual}} q_i^t - \lambda_{\text{col}} \mathbf{1}_{\text{col},i}^t - \lambda_{\text{imp}} \kappa_i^t - \lambda_{\text{lazy}} \mathbf{1}_{\text{lazy},i}^t, \quad (9)$$

where $\Delta d_i^t = d_i^{t-1} - d_i^t$, $d_i^t = \|\mathbf{p}_i^t - \mathbf{p}_e^t\|_2$, and κ_i^t denotes collision-impact intensity.

To stabilize cooperation under zero communication, CGCA introduces locality-aware directional gating:

$$g_{\text{dir}}(d) = \begin{cases} 1, & d \leq 40 \text{ m}, \\ \frac{80-d}{40}, & 40 < d \leq 80 \text{ m}, \\ 0, & d > 80 \text{ m}. \end{cases} \quad (10)$$

Capture-share credit is hard-gated outside 60 m and weighted by closing behavior. Define closing speed $v_{i,\text{clo}}^t = -\dot{d}_i^t$. The raw contribution is

$$\tilde{c}_i^t = \mathbf{1}[d_i^t \leq 60] \left(\alpha_p e^{-d_i^t/d_0} + \alpha_v [v_{i,\text{clo}}^t]_+ + \alpha_r \mathbf{1}[d_i^t \leq R_c] \right), \quad (11)$$

and the normalized share is

$$\hat{c}_i^t = \frac{\tilde{c}_i^t}{\sum_{j=1}^{N_t} \tilde{c}_j^t + \epsilon}. \quad (12)$$

To suppress free-rider behavior, a participation ratio multiplies global capture reward:

$$\eta_i^t = \mathbf{1}[d_i^t \leq 60] \mathbf{1}[v_{i,\text{clo}}^t > 0.5], \quad \rho^t = \min\left(1, \frac{\sum_i \eta_i^t}{0.5N_t}\right). \quad (13)$$

Thus, if fewer than half of alive pursuers actively close the target, collective capture bonus is proportionally downscaled.

Collision suppression is explicitly encoded as

$$\mathbf{1}_{\text{col},i}^t = \mathbf{1}_{\text{obs-hit},i}^t + \mathbf{1}_{\text{team-hit},i}^t + \mathbf{1}_{\text{shield},i}^t, \quad (14)$$

which penalizes obstacle impacts, inter-agent contacts, and safety-shield triggers in a unified term.

The 40/60/80 m thresholds are chosen to align with the 60 m sensing extremum in Stage 5 and the practical maneuver envelope of the platform: 40 m acts as high-confidence local-interaction core, 60 m matches reliable observability scale, and 80 m suppresses non-contributive far-field reward leakage.

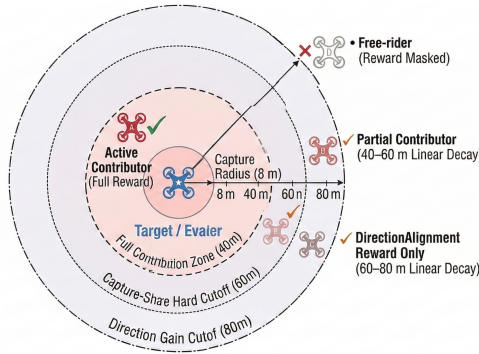


Fig. 3. Contribution-Gated Credit Assignment. Direction reward is fully active within 40 m, decays over 40–80 m, and vanishes beyond 80 m; capture-share is hard-gated beyond 60 m. This local credit geometry suppresses free-rider equilibria in zero-communication team pursuit.

V. EXPERIMENTS AND EVALUATIONS

A. Setup and baselines

Evaluation follows the provided Stage-5 protocol (main benchmark: 3 seeds, 500 episodes/seed; robustness suites: 200 episodes/setting/seed, with delay using 4–5 evaluation seeds). Baselines include FULL OBS, EUCLIDEAN, LOCAL-NO-GATE, CTDE MAPPO, and APF+PN.

Comparisons are intentionally factorized. OURS-LITE, FULL OBS, and LOCAL-NO-GATE belong to the same inherited parameter-shared decentralized PPO family; OURS-LITE vs. FULL OBS isolates information-structure effects (50-D parsimonious vs. 83-D team-coupled), and OURS-LITE vs. LOCAL-NO-GATE isolates the role of CGCA under the same 50-D setting. CTDE MAPPO is treated separately as a centralized-critic baseline to contrast centralized coupling against decentralized execution in this task.

B. Curriculum maturation and visibility gating

To clarify where search capability originates, we adopt a stage-wise curriculum with explicit *visibility gating*. During training, target observability is conditionally released only

when either the explored-space ratio exceeds a stage-specific threshold τ or a hard episode timeout is reached (> 1500 steps in the late-stage setting). The threshold τ is progressively increased with curriculum maturation: Stage 1 has no gating, while later blind-search stages tighten from 45% (Stage 3) to 60% (Stage 4) and 70% (Stage 5).

This mechanism creates a structural bottleneck: agents must first internalize 3D exploration before reliable tracking signals become available. In other words, observability is earned through coverage rather than granted a priori, which prevents early lucky sightings from dominating learning. Critically, this gate is *only active during training* as an inducement for tactical emergence; it is fully removed during evaluation, where policies are tested without artificial visibility constraints.

C. Training dynamics and sample efficiency

Fig. 1 shows that OURS-LITE reaches the high-return regime earlier and with lower oscillation amplitude than FULL OBS and CTDE MAPPO. A key reason is representation-level compression: removing 33 dimensions of delay-sensitive team-coupling features shrinks the actor input manifold and reduces nuisance covariance under delayed observations. In PPO, the policy-gradient estimator

$$\hat{g}_t = \nabla_{\theta} \log \pi_{\theta}(a_i^t | \mathbf{o}_i^t) \hat{A}_i^t \quad (15)$$

can be interpreted through a policy-input variance lens: fewer delay-sensitive channels reduce nuisance covariance, which is consistent with empirically more stable policy updates and improved sample efficiency in our curriculum. In contrast, CTDE MAPPO shows less stable value-learning dynamics in this setting: the 338-D centralized critic may increase approximation burden and potentially amplify distribution-shift sensitivity once visibility gates and clutter-induced mode switches become active.

Importantly, the middle panel of Fig. 1 (Clean Win Rate) shows that CTDE MAPPO is not weak from the outset: in simpler curriculum phases (Stage 1–2), it stays above 90% for a continuous 2M-step interval before Stage 3. Instability emerges mainly at the Stage-3 transition, where severe 3D non-convex occlusions and visibility gating are introduced. These observations suggest that centralized critics may become fragile when high-dimensional value approximation and abrupt visibility-induced distribution shift occur simultaneously.

Why may CTDE MAPPO become unstable here? The centralized critic consumes 338-D input, which may intensify approximation difficulty in highly non-convex 3D clutter. Meanwhile, visibility-gated phase transitions induce abrupt observation-distribution shifts, potentially amplifying critic-target variance and gradient jitter. The combined evidence is consistent with unstable value learning and weaker policy improvement despite centralized conditioning.

D. Main benchmark and ablation study

Within the decentralized parameter-shared PPO family, OURS-LITE vs. FULL OBS isolates the effect of information structure: removing explicit teammate-coupled channels

TABLE III

MAIN STAGE-5 BENCHMARK (MEAN \pm STD OVER 3 SEEDS, 500 EPISODES/SEED). OURS-LITE, FULL OBS, AND LOCAL-NO-GATE ARE INHERITED PARAMETER-SHARED DECENTRALIZED PPO-FAMILY VARIANTS.

Method	Success	Clean	Collision	Avg Steps
OURS-LITE	0.753\pm0.091	0.752\pm0.091	0.223\pm0.066	683.6 \pm 269.4
FULL OBS	0.721 \pm 0.071	0.721 \pm 0.072	0.253 \pm 0.089	655.4\pm106.7
EUCLIDEAN	0.586 \pm 0.120	0.583 \pm 0.121	0.353 \pm 0.092	887.9 \pm 237.7
LOCAL-NO-GATE	0.569 \pm 0.090	0.568 \pm 0.089	0.389 \pm 0.106	669.1 \pm 223.2
CTDE MAPPO	0.006 \pm 0.004	0.006 \pm 0.004	0.159 \pm 0.111	2806.8 \pm 139.1
APF+PN	0.125 \pm 0.007	0.125 \pm 0.007	0.875 \pm 0.007	124.9 \pm 2.0

improves success (0.753 vs. 0.721) and reduces collisions (0.223 vs. 0.253). This supports the hypothesis that richer coupling is not always more robust under delayed/noisy pursuit.

Ablation insight (OURS-LITE vs. LOCAL-NO-GATE). Removing CGCA under the same 50-D zero-communication setting causes an 18.4-point success drop (0.753 \rightarrow 0.569) and a 16.6-point collision increase (0.223 \rightarrow 0.389). This isolates CGCA as a necessary mechanism rather than a cosmetic regularizer.

E. Kinematic stress tests

Fig. 4 shows speed sweep (7.0–10.0 m/s), where OURS-LITE degrades gracefully from 0.907 to 0.790 success. EUCLIDEAN exhibits the classic kinematic trap: straight-line chasing delays feasible turn commitment in clutter, causing overshoot-recovery loops and inflated episode length.

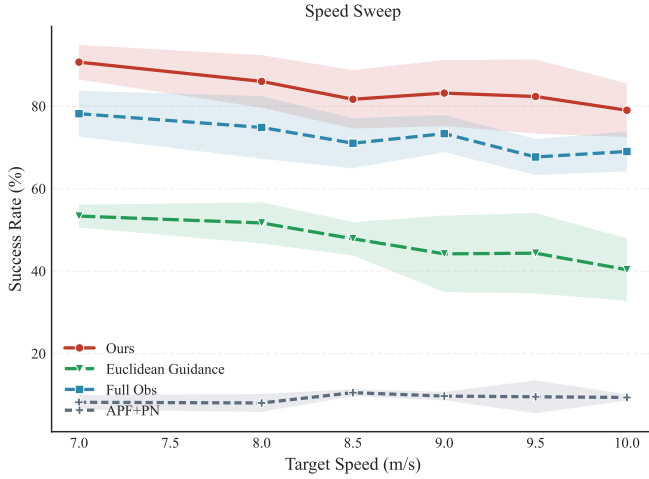


Fig. 4. Velocity sweep. OURS-LITE maintains the strongest success–collision trade-off under increasing evader speed, while EUCLIDEAN suffers persistent high-step inefficient pursuits.

Fig. 5 reports yaw-cap restriction (0.8 \rightarrow 0.2 rad/s). Under severe turning limits, performance drop reflects algorithm–physics mismatch: reactive corrections arrive too late when feasible arc space collapses.

F. Sim-to-real robustness

Noise and delay robustness are shown in Fig. 6 and Fig. 7. Under delay, FULL OBS degrades more sharply than OURS-LITE, which is consistent with state de-synchronization:

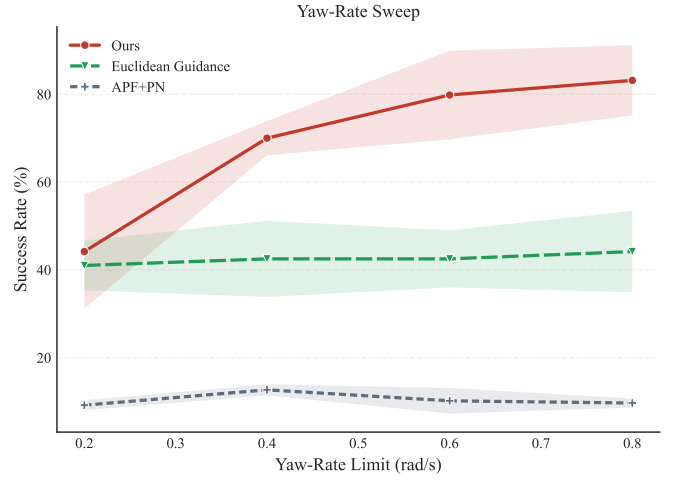


Fig. 5. Yaw-rate sweep. The proposed configuration preserves a robust mid-regime margin and shows graceful degradation as maneuver authority shrinks.

densely coupled teammate channels may propagate stale estimates and potentially amplify control-error cascades.

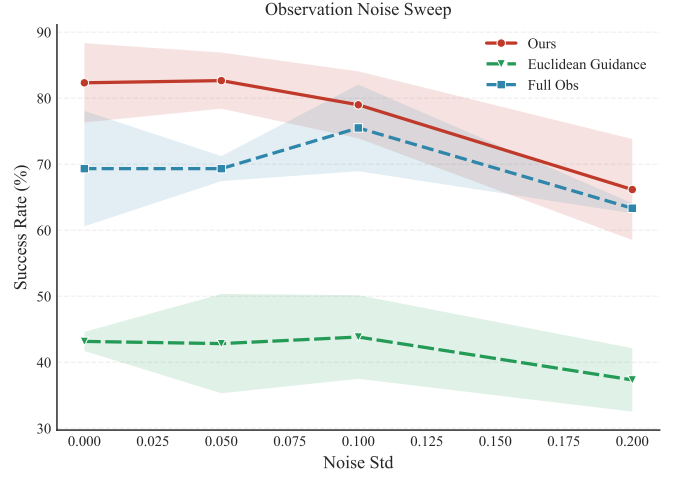


Fig. 6. Observation-noise sweep ($\sigma \in [0, 0.20]$). OURS-LITE remains strongest across all tested noise levels.

G. Qualitative analysis: cross-layer vertical sweep

Fig. 8 reveals a three-phase maneuver pattern rather than a single reactive chase. *Initial Search*: guided by the shared 3D A* prior, agents fan out to frontier-consistent corridors while preserving safety spacing. *Altitude Stratification*: once target likelihood concentrates, one pursuer climbs to the upper low-occupancy band and the remaining agents occupy mid/low bands, exploiting measured anisotropy (15.9%/12.1%/10.2%) to reduce vertical escape options. *Topological Containment*: the formation then uses obstacle morphology—especially U-shaped walls and corner pockets—as virtual teammates, tightening a cross-layer envelope until terminal capture.

This phased behavior explains why communication-free coordination remains effective: agents do not exchange explicit messages, yet shared topology priors and CGCA-induced local

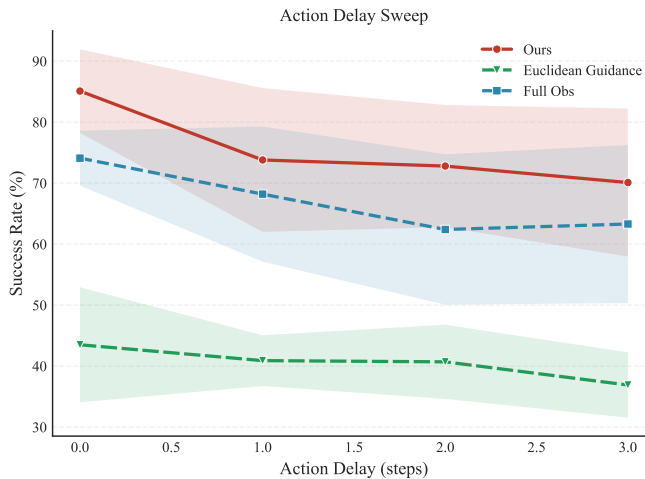


Fig. 7. Action-delay sweep (0–3 steps). OURS-LITE preserves the best absolute robustness profile under latency perturbation.

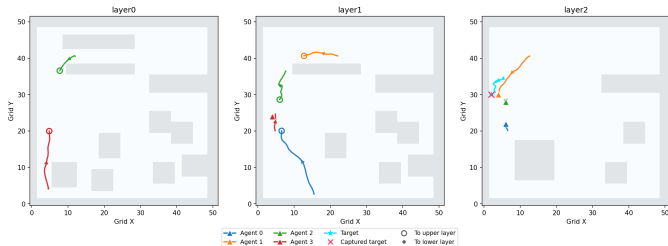


Fig. 8. 3D Z-axis tactical slicing. The team performs cross-layer vertical sweep: upper-layer pressure constrains vertical escape while lower-layer agents close horizontal corridors, yielding a communication-free topological enclosure.

incentives synchronize role allocation over time. Importantly, the enclosure trajectory is geometrically consistent with the map’s layered free-space structure, indicating true 3D tactical organization rather than incidental altitude jitter.

VI. ZERO-SHOT GENERALIZATION ON PROCEDURALLY GENERATED URBAN CANYONS

To test map over-fitting, we evaluate OURS-LITE zero-shot on five procedurally generated *Urban Canyon* maps with obstacle densities 0.08–0.24. The generator uses connected 2.5D anisotropic street-corridor layouts (rather than random voxel noise), yielding physically meaningful maneuver corridors and controlled topology shift.

As shown in Fig. 9, performance degrades gracefully with density: at the hardest map (0.24), success remains around 61% while collision stays below 40%, and average steps remain in the 350–450 band. These trends are consistent with structural transfer (cross-layer containment under vertical anisotropy) rather than fixed-map memorization.

VII. DISCUSSION AND LIMITATIONS

The empirical picture supports a robustness-oriented design principle: in communication-constrained multi-robot pursuit, less cross-agent coupling can sometimes yield more reliable coordination. In our setting, the 83-D team-coupled profile is

outperformed by the 50-D parsimonious profile, and cooperation quality is maintained by locality-aware CGCA without explicit communication. This combination is consistent with the view that stale coupling channels may introduce harmful variance under delay/noise, whereas sparse local signals can remain controllable.

Two limitations remain. First, yaw-restriction sweeps currently do not include FULL OBS, so low-yaw cross-method comparisons are incomplete. Second, the present noise suite is bounded at $\sigma \leq 0.20$; stronger perturbation regimes are needed for firmer conclusions under extreme sensing corruption.

VIII. CONCLUSION

Built on the inherited path-guided decentralized scaffold of [1], this paper studies a different question from framework design: robustness-oriented information and credit structure in communication-constrained 3D pursuit–evasion. The results support two linked findings: (i) richer team-coupled observations are not always better, and representational parsimony can improve robustness; (ii) communication-free coordination can remain effective when local credit assignment is properly structured through CGCA. Across benchmark, stress, and zero-shot urban-canyon transfer evaluations, the evidence indicates a practical design principle rather than a universal rule: in communication-constrained multi-robot pursuit, reducing explicit cross-agent coupling can sometimes yield more robust coordination.

REFERENCES

- [1] J. Ying, Z. Li, Z. Dong, G. Wu, and Y. Liao, “Generalizable Collaborative Search-and-Capture in Cluttered Environments via Path-Guided MAPPO and Directional Frontier Allocation,” *arXiv preprint arXiv:2512.09410*, 2025.
- [2] R. Lowe *et al.*, “Multi-agent actor-critic for mixed cooperative-competitive environments,” in *Advances in Neural Information Processing Systems*, 2017.
- [3] J. Foerster, G. Farquhar, T. Afouras, N. Nardelli, and S. Whiteson, “Counterfactual multi-agent policy gradients,” in *AAAI Conference on Artificial Intelligence*, 2018.
- [4] C. Yu *et al.*, “The surprising effectiveness of PPO in cooperative multi-agent games,” in *NeurIPS Datasets and Benchmarks*, 2022.
- [5] S. Sukhbaatar, A. Szlam, and R. Fergus, “Learning multiagent communication with backpropagation,” in *Advances in Neural Information Processing Systems*, 2016.
- [6] J. Jiang and Z. Lu, “Learning attentional communication for multi-agent cooperation,” in *Advances in Neural Information Processing Systems*, 2018.
- [7] A. Das, T. Gervet, J. Romoff, D. Bouchard, L. V. Belanger, and J. Pineau, “TarMAC: Targeted multi-agent communication,” in *International Conference on Machine Learning*, 2019.
- [8] Y. Jiang, Y. Guo, and S. Li, “Graph convolutional reinforcement learning for multi-agent cooperation,” in *International Conference on Learning Representations Workshop*, 2020.
- [9] P. Sunhag *et al.*, “Value-decomposition networks for cooperative multi-agent learning,” in *International Conference on Autonomous Agents and Multiagent Systems*, 2018.
- [10] T. Rashid *et al.*, “QMIX: Monotonic value function factorisation for deep multi-agent reinforcement learning,” in *International Conference on Machine Learning*, 2018.
- [11] P. E. Hart, N. J. Nilsson, and B. Raphael, “A formal basis for the heuristic determination of minimum cost paths,” *IEEE Transactions on Systems Science and Cybernetics*, vol. 4, no. 2, pp. 100–107, 1968.
- [12] O. Khatib, “Real-time obstacle avoidance for manipulators and mobile robots,” *The International Journal of Robotics Research*, vol. 5, no. 1, pp. 90–98, 1986.

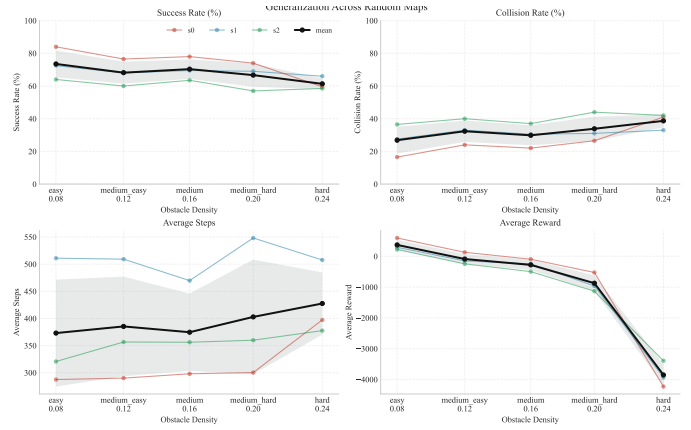
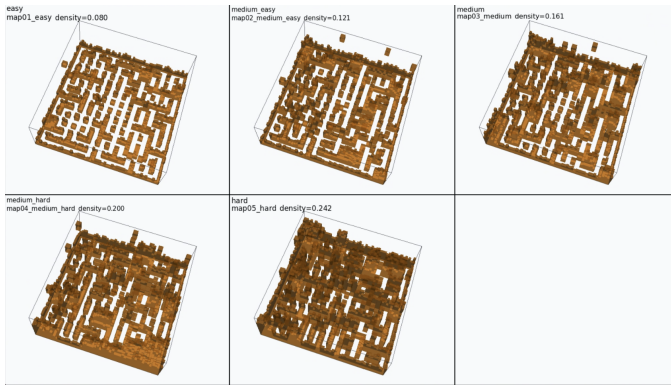


Fig. 9. Zero-shot transfer on five unseen Urban Canyon maps (density 0.08–0.24). **Left:** map examples from easy to hard density. **Right:** seed-wise and mean success, collision, average steps, and reward without fine-tuning. OURS-LITE degrades gracefully with density, remaining near 61% success and below 40% collision at density 0.24, consistent with structural transfer rather than fixed-map memorization.

[13] P. Zarchan, *Tactical and Strategic Missile Guidance*, 6th ed. Reston, VA, USA: AIAA, 2012.

[14] F. Sadeghi and S. Levine, “CAD²RL: Real single-image flight without a single real image,” in *Robotics: Science and Systems*, 2017.

[15] L. Busoniu, R. Babuska, and B. De Schutter, “A comprehensive survey of multiagent reinforcement learning,” *IEEE Transactions on Systems, Man, and Cybernetics, Part C*, vol. 38, no. 2, pp. 156–172, 2008.